Applied Thermal Engineering 258 (2025) 124566

Contents lists available at ScienceDirect

Applied Thermal Engineering

journal homepage: www.elsevier.com/locate/ate

Research Paper

Energy conversion mechanisms in turbomachines for high-temperature endothermic reactions: Redefining energy quality

Dylan Rubini [a,*], Budimir Rosic [a], Liping Xu [b]

[a] Oxford Thermofluids Institute, Department of Engineering Science, University of Oxford, Oxford OX2 0ES, UK
[b] Whittle Laboratory, Department of Engineering, University of Cambridge, Cambridge CB3 0DY, UK

ARTICLE INFO

Keywords:
Turbomachinery
Endothermic chemical processes
Steam cracking
Turbo-reactor
Loss breakdown

ABSTRACT

A new class of turbomachines, called turbo-reactors, have emerged to decarbonize high-temperature chemical processes. These applications unlock a new aerothermochemical design space for turbomachines. This paper explains how the turbo-reactor has the potential to be a "chemically tuned" device. In contradiction with conventional design wisdom, this can be achieved by balancing entropy generation within the flow against heat absorption by the reaction. This enables the "design" of a reaction-efficient temperature profile. To do this, it is necessary to understand and quantify the distribution of the entropic and isentropic mechanisms responsible for energy conversion. This paper uses high- and low-fidelity computations to decompose the energy conversion process into mechanisms based on a spatial decomposition. A range of Mach and Reynolds number regimes are studied, as well as a multistage configuration without vaneless space. The energy conversion breakdown analysis indicates that the entropic energy conversion dominates over the isentropic component with a contribution of 65%. The dominant source of entropy production is viscous dissipation generated by the thick diffuser trailing edge, accounting for 25% of the total. The shock system provides 20% of the energy conversion, almost entirely due to reversible pressure rise rather than entropy production. The energy conversion coefficient is independent of Reynolds number over engine-relevant conditions, whereas Mach effects are more significant. Across the Mach numbers range 1.1 to 1.5, the energy conversion coefficient increases by 20%. This is lower than expected as a result of the opposing effects of reversible and irreversible energy conversion contributions.

1. Introduction

1.1. Historical perspective, motivation and background

The fundamental principles of turbomachinery design have been shaped to minimize the degradation of energy quality, *i.e.,* the exergy destruction or lost work potential, during energy conversion processes in power generation, aviation and industrial processes [1,2]. The focus on reducing energy quality degradation (and increasing fuel efficiency) intensified following the 1970s oil crisis, reaffirming that the finite fossil fuel resource was rapidly depleting, and encouraging industries to strive towards extracting the maximum utilizable work, that is, the exergy, from nonrenewable energy resources. Today, the drive to minimize aerodynamic losses for efficiency gains is ubiquitous in turbomachinery [3].

In the context of conventional compressors (*i.e.,* energy-imparting machines), the bladed flow path is designed to maintain the absorbed shaft power in the form of pressure or kinetic energy to preserve energy quality. However, now with the emergence of new applications for turbomachines — decarbonizing high-temperature endothermic reaction processes with a new turbo-reactor [4,5] — this is no longer the case. Specifically, the goal of the turbo-reactor seen in Fig. 1 is to convert energy from the electric-motor-powered shaft into internal energy of the fluid (not pressure). Since there is no global pressure rise, this can be achieved effectively and without instability using ultrahigh-loading rotating blades to impart mechanical energy to the fluid before it is dissipated (and converted) into internal energy. The working fluid undergoes a chemical reaction along most of the bladed flow path, which presents a new set of requirements for the design. That is, the imparted mechanical energy must be dissipated at a rate determined by the reaction, which is typically relatively fast. This means that enhanced entropy generation is not only unavoidable but necessary. This new turbomachinery design principle of leveraging entropy generation for ultrafast energy transformation along the bladed path is fundamentally different from conventional wisdom.

1.2. Objectives of this paper

Following a recap of the basic requirements and key features of the turbo-reactor concept that has been introduced in detail in previous

* Corresponding author.
E-mail address: dylan.rubini@eng.ox.ac.uk (D. Rubini).

https://doi.org/10.1016/j.applthermaleng.2024.124566
Received 17 June 2024; Received in revised form 12 September 2024; Accepted 4 October 2024
Available online 16 October 2024

Nomenclature

Roman Letters

b_{true}	True diffuser chord length, m
c_p	Isobaric heat capacity, $\text{J kg}^{-1}\text{ K}^{-1}$
C_x	Diffuser axial chord length, m
h_0	Total enthalpy, J kg^{-1}
p	Static pressure, bar
t_{TE}	Diffuser trailing edge thickness, m
T	Static temperature, K
u_i	Velocity vector, m s^{-1}
U	Mean blade speed, m s^{-1}
V_1	Diffuser inlet velocity, m s^{-1}
w	Diffuser blade pitch, m

Greek Letters

ζ_h	Total energy conversion coefficient
$\zeta_{h,\text{rev.}}$	Reversible (isentropic) energy conversion coefficient
$\zeta_{h,s}$	Irreversible (entropic) energy conversion coefficient
μ	Dynamic molecular viscosity, Pa s
ρ	Density, kg m^{-3}
$\bar{\tau}_{ij}$	Mean flow shear stress tensor, Pa
τ^R_{ij}	Reynolds stress tensor, Pa

Dimensionless Groups

M	Mach number
Re	Reynolds number
σ	Shock function, $\frac{\boldsymbol{M}\cdot\nabla p}{\lvert\nabla p\rvert}$

Superscripts

$\square'$	Fluctuating component
$\overline{\square}$	Time averaged

Acronyms

BL	Boundary layer
ITV	Integrated turning vane
LES	Large-eddy simulation
LE/TE	Leading/trailing edge
PS/SS	Pressure/suction surface
SWBLI	Shockwave boundary layer interaction
URANS	Unsteady Reynolds–averaged Navier–Stokes

work by the authors [4–7], the paper is organized into four distinct parts summarized below.

(1) The reaction requirements are outlined along with how the turbo-reactor is designed to achieve them.
(2) The consequences of converting electricity to heat and thus degrading energy quality are clarified. By introducing chemical exergy as a new vector of energy quality for turbomachines, it will be demonstrated that this process is sensible from a thermodynamic perspective.
(3) This paper demonstrates how the turbo-reactor can be designed as a "chemically reaction tuned" — or for brevity, a "chemically tuned" — device (and is not a "bad compressor" or a "mixer"). It is explained how aerodynamic losses can be exploited to design a reaction-efficient temperature profile by controlling the dissipation profile. This unlocks a new dimension within the design space of turbomachines.
(4) To design this reaction-efficient temperature profile, an improved understanding of the energy conversion mechanisms is required. Therefore, the distribution of energy conversion mechanisms is numerically investigated over a range of design conditions. An improved understanding of this process will inform future aerodynamic design optimization to tune the energy conversion process for increased reaction efficiency.

The focus of this paper is on reacting flow applications. For context, the example endothermic reaction application of steam cracking of hydrocarbon feedstocks [4,5] is used. However, Rubini et al. [7] demonstrated that the turbo-reactor can also be used to decarbonize a variety of other endothermic reaction processes. The reader is referred to Chauhan et al. [8], Mynko et al. [9], and Thiel & Stark [10] for a comprehensive review of alternative pathways to decarbonize high-temperature chemical reaction processes, which include electrochemical pathways, alternative combustion fuels such as hydrogen, plasma pyrolysis, and electric furnaces using resistance (Joule) heating.

2. Decarbonizing endothermic reactions: The turbo-reactor concept

The renewably-powered turbo-reactor replaces fossil-fuel-fired tubular furnaces. For an ethane feedstock, Fig. 2(*a*) compares a typical turbo-reactor stage with a small section of a furnace pipe of equivalent length. In the furnace tube, the rate of energy transfer is limited by the thermal diffusion timescale of surface heat exchange. Moving to direct volumetric energy input within the turbomachine (see Fig. 2), the energy transfer rate is instead driven by the rotor convection timescale. Whereas the thermal diffusion timescale is essentially fixed, the convection timescale can be compressed through high supersonic flow speeds, as is done in the turbo-reactor. Therefore, orders of magnitude higher power densities can be achieved relative to conventional furnaces (see Fig. 2(*a*) & (*e*)).

2.1. Reaction requirements

For turbo-reactor-powered endothermic chemical reaction processes, value is created by chemically transforming low-value feedstock (*e.g.* ethane) into higher-value products (*e.g.,* ethylene). Alongside power input and power density targets, the efficiency of this chemical transformation — that is, the fraction of feedstock that is converted into high-value product species — is the most important figure of merit and displaces isentropic stage efficiency as the driving design metric for this new class of machines. Achieving a highly efficient chemical reaction requires two design features, both of which are now possible by replacing furnaces with the turbo-reactor.

(1) The reaction should progress uniformly in the pitchwise and spanwise directions. The progress of the reaction is most significantly impacted by the temperature field. In the pipes of conventional furnaces, Fig. 2(*c*) illustrates that the temperature distribution is highly nonuniform due to heat transfer through the walls. This results in reaction progression along each streamline going out of sync, as shown by the radial ethane feed conversion difference ΔY_C highlighted in Fig. 2(*d*). This leads to poor reaction efficiency and solid carbon (*i.e.,* coke) forming directly on the metal surface. Fundamentally, this challenge of nonuniformity cannot be avoided even with novel electric or hydrogen furnaces [11], which are still surface heat exchangers. In contrast, in the turbo-reactor, the volumetric energy input mechanism combined with turbulent mixing between stages facilitates a significantly more uniform temperature distribution (see Fig. 2(*b*)). This can promote higher reaction efficiency.

Fig. 1. A turbo-reactor render showing some example industries that it could decarbonize.

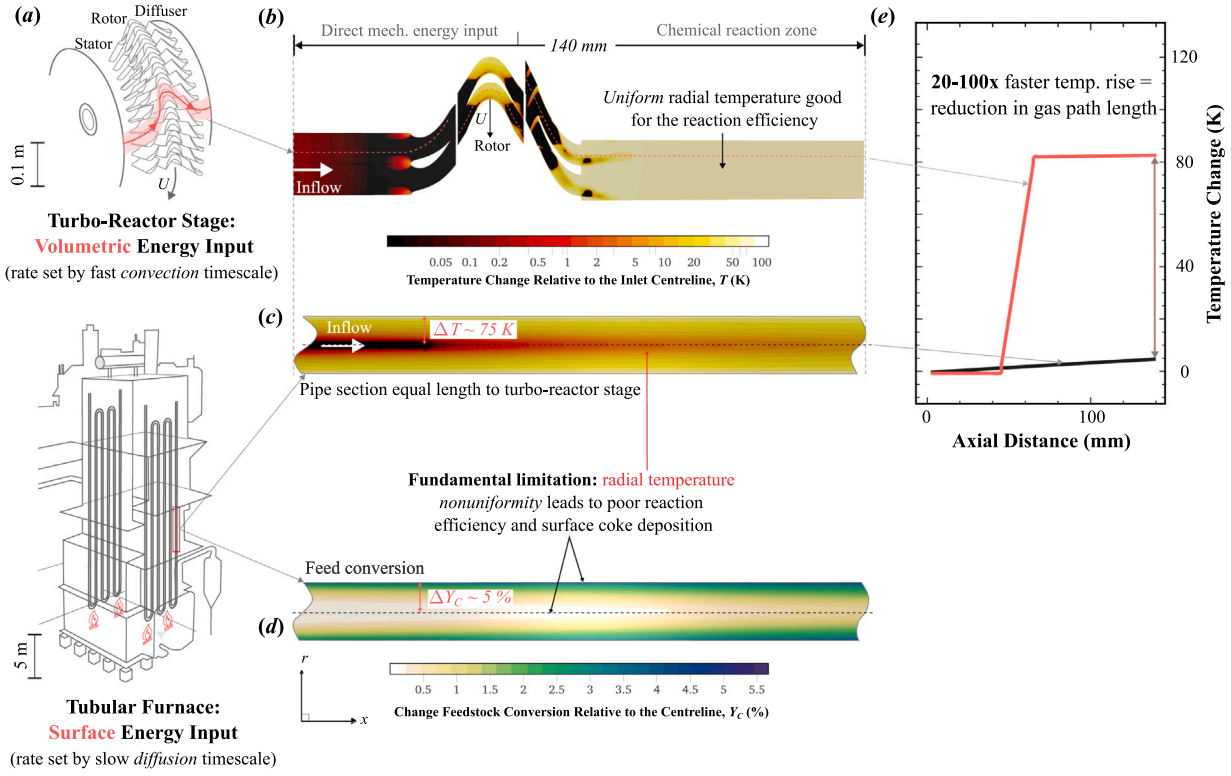

Fig. 2. (*a*) Schematic comparison between a turbo-reactor stage and a typical steam cracking furnace pipe (*b*) & (*c*) a comparison of the static temperature change on a *logarithmic* scale (*d*) change in ethane feedstock conversion change and (*e*) a comparison of the averaged axial temperature change.

(2) To increase reaction efficiency, shorter reaction timescales at higher static temperature levels should be designed for, as shown in Fig. 3. Bypassing metallurgical limitations due to the hot walls of conventional surface heat exchanges allows the turbo-reactor to achieve higher bulk fluid temperatures over a shorter reaction timescale. This improvement in reaction efficiency is a key advantage of the turbo-reactor that is not possible with surface-heat-exchange-based methods to decarbonize high-temperature chemical processes (*e.g.,* hydrogen or electric furnaces) [11].

We will see that these features of the turbo-reactor design are enabled by controllably enhancing aerodynamic losses and viscous dissipation.

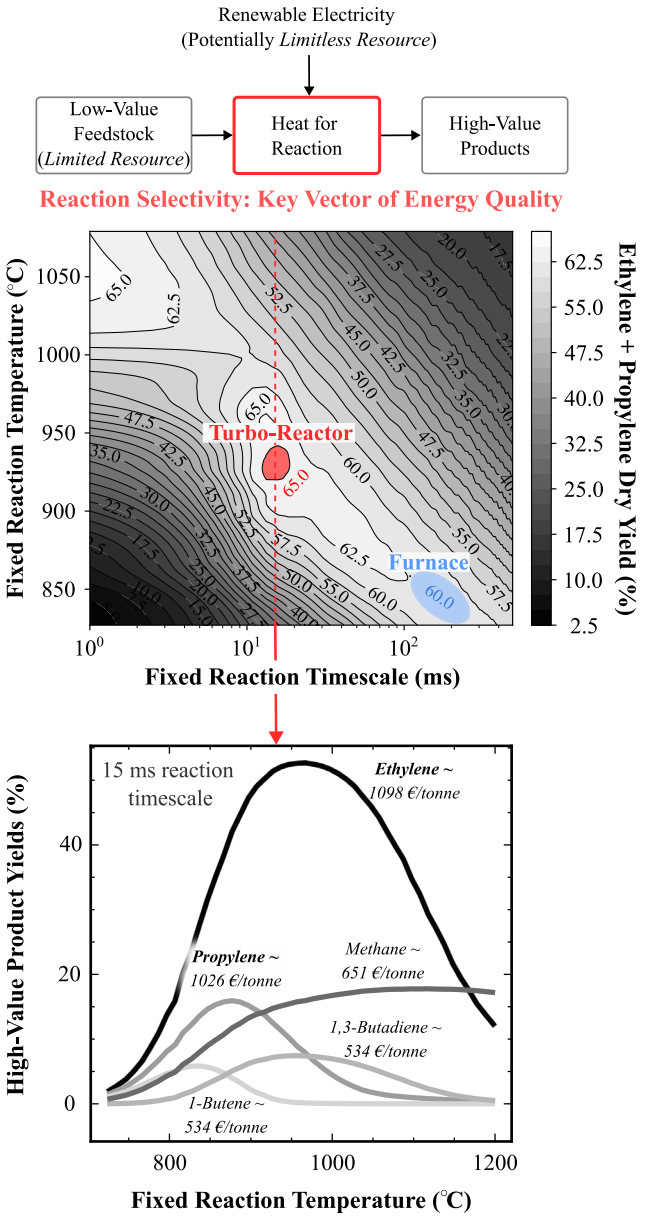

Fig. 3. Idealized dry yields of selected products as a function of fixed reaction temperature and timescale. The lower figure show the product yields as a function of temperature at a fixed reaction timescale 25 ms as highlighted by the red dashed line.

The next section summarizes the elemental stage design philosophy and approach to configuring the multistage environment to achieve the reaction requirements presented in this section.

2.2. Working principles of the turbo-reactor

2.2.1. Energy transfer

Short reaction timescale requirements dictate that an ultrahigh loading impulse rotor is employed. Since there is no requirement for a global pressure gain, it is possible to develop supersonic rotor blades with a work coefficient of up to $\psi = \frac{\Delta h_0}{U^2} \approx 8.0$, depending on the fluid properties [7]. This is 20 times that of an axial compressor. Without a global pressure rise, efficiency and stability restrictions that limit the work coefficient in compressors are alleviated [12], enabling this loading level.

2.2.2. Energy conversion

To supply an enthalpy dh to the chemical reaction at a constant pressure, the Gibbs equation

$$dh = \frac{1}{\rho} dp + T ds \tag{1}$$

implies that an entropy change ds must be produced to satisfy the constant global static pressure ratio ($dp \approx 0$) boundary conditions. Since the designer is no longer concerned with efficiency, aerodynamic losses (and hence entropy production and viscous dissipation) can be leveraged to control the energy conversion rate profile to design a temperature profile that favors optimal reaction dynamics (see Section 3.1).

2.2.3. Chemically tuning the interstage vaneless space

Fig. 4 shows that each stage is separated by an interstage vaneless mixing space where the mechanical energy absorbed through the rotor is converted into internal energy. This energy conversion process must be distributed over a series of stages to counterbalance the drop in temperature due to the endothermic chemical reaction, as shown in Fig. 5. In Fig. 3 it was suggested that the local residence time favored by the reaction varies with the temperature level, which is different for each stage. Therefore, the local residence time can be controlled by varying the length of the vaneless space between stages (L). This becomes a new tunable control parameter (see Fig. 4), which can be customized stage by stage from length 0 to NC_x to design a reaction-efficient temperature profile (see Fig. 5). Furthermore, this vaneless mixing space is also critical to allow thermochemical nonuniformities to mix-out. The design of the temperature profile for efficient chemistry is explained in more detail in Section 3.1.

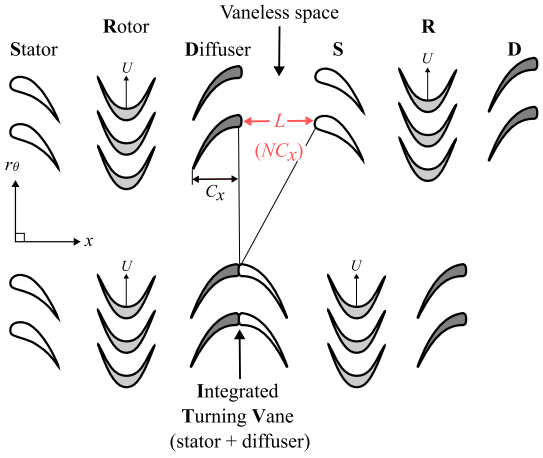

Fig. 4. Variable interstage vaneless space length from 0 diffuser chords (C_x), *i.e.,* an integrated turning vane, up to NC_x.

For preheating the gas mixture before reaction activation, there are no reaction timescale requirements, so a "compact stage" design can be used. This is achieved by combining the stator and diffuser into an integrated turning vane (ITV), as shown in Fig. 4.

2.3. New vector of energy quality (Exergy)

It is evident that the chemical processes driven by the turbo-reactor rely on *irreversibilities* to rapidly dissipate mechanical energy within the required rapid reaction timescales (see Fig. 3) while promoting reaction uniformity (and hence performance). Therefore, it is important to assess the thermodynamic implications of this degradation of energy quality (exergy).

Before doing so, a new vector of energy quality must be introduced for this new class of turbomachines. Conventionally, turbomachinery design practice concentrates only on *physical* exergy. However, in the new endothermic reaction applications, energy is supplied to a chemical reaction along the bladed flow path. This means that *chemical*

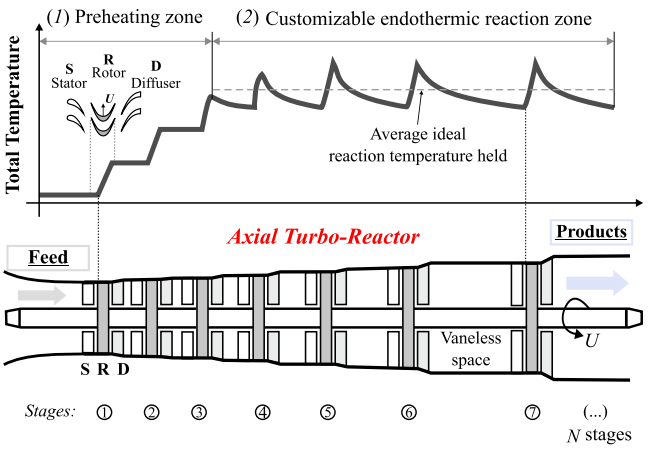

Fig. 5. Schematic of the elemental stage and multistage environment for the turbo-reactor, illustrating a typical total temperature profile for an endothermic chemical process.

exergy, defined in Appendix, must be considered in addition to physical exergy as a new vector of energy quality. This is an entirely new design consideration for turbomachines.

Equipped with chemical exergy, as well as the price of energy and the cost of feed/products, the impact of exploiting viscous dissipation can be understood using Fig. 6. The chemical exergies are calculated using the equations presented in Appendix. The inlet & output mass fraction distributions and reaction irreversibility are calculated from 1D plug-flow reactor chemical kinetic calculations. Aerodynamic irreversibility is determined by the predicted entropy generation from CFD calculations, and motor & heat losses are set to typical values for turbomachines. The energy price and the cost of the feedstock & products are estimated from the current (2024) average electricity prices and average hydrocarbon market prices [13], respectively. The energy requirement is set to that needed for the preheating and reaction completion.

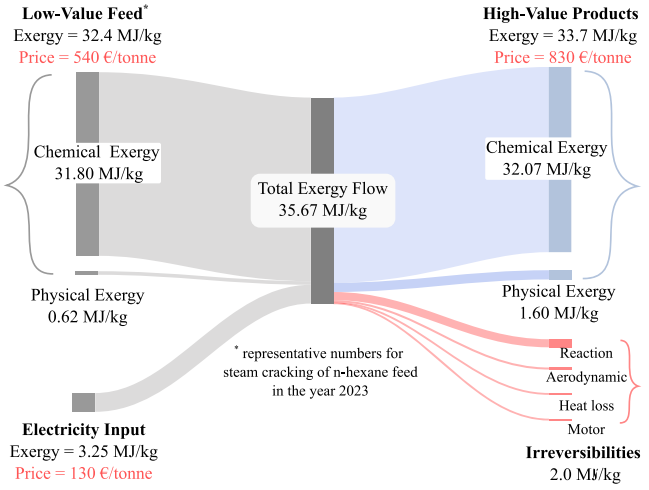

Fig. 6. Sankey diagram showing an exergy balance for a representative steam cracker with an n-hexane feed in 2023.

Fig. 6 shows that the supplied electricity has a significantly lower cost and exergy content compared to the feedstock. Therefore, based on the values in Fig. 6, combined with the assumption that the electricity supplied is semi-limitless (*i.e.,* provided by renewable energy), it is reasonable to sacrifice the energy quality supplied to the turbo-reactor by developing irreversibilities. This enables higher reaction efficiencies. After all, a higher reaction efficiency means more species in the effluent gas stream that have a high value. Therefore, it is useful to view reaction efficiency as a new vector of energy quality.

3. Leveraging aerodynamic losses for a controllable energy conversion profile

3.1. Chemically-tuned turbomachines: Design of a reaction-efficient temperature profile

In Section 2 it was highlighted that at the global *coarse-grained* level, the turbo-reactor is designed to operate at a higher temperature level over shorter timescales to improve reaction efficiency. We saw that the temperature could be controlled at the coarse-grained stage-level (see Section 2.2.3) by customizing the interstage vaneless space distance.

At the *fine-grained* level, there is not only an optimal reaction temperature level and timescale, but also an ideal temperature profile that benefits reaction performance. This section explains how the local energy conversion process, and thus the profile of energy absorbed by the reaction, could be tuned to "design" an ideal reaction-efficient temperature profile. The ability to perform temperature profiling is an important benefit of distributing energy addition across a series of stages. We will explore the potential benefits of tailoring the energy conversion profile at a fine-grained level, opening new possibilities for future aerothermochemical design optimization. The following discussion will be structured following the three boxes displayed in Fig. 7.

3.1.1. Box ①: Objectives

In an idealized scenario, the temperature level is raised and maintained (see Fig. 7) at an ideal reaction temperature set by the given residence time (see Fig. 3). To better understand how to design for this reaction temperature profile, it is useful to consider the temperature transport equation for the time-averaged base flow [14]. For an ideal gas in simplified form, this is defined as follows:

$$\bar{\rho}c_p\frac{D\bar{T}}{Dt} \equiv \bar{\rho}c_p\bar{u}_j\frac{\partial\bar{T}}{\partial x_j} \approx \underbrace{\lambda_{eff.}\frac{\partial^2\bar{T}}{\partial\bar{x}_j^2}}_{\text{diffusion}} + \Bigg(\underbrace{\bar{u}_i\frac{\partial\bar{p}}{\partial x_i}}_{\text{pressure work}} + \underbrace{(\bar{\tau}_{ij}+\tau_{ij}^R)\frac{\partial\bar{u}_i}{\partial x_j}}_{\text{viscous work}} \Bigg) - \underbrace{\dot{\omega}_T}_{\text{heat sink}} \tag{2}$$

where $\bar{\rho}$ is the density, c_p is the isobaric heat capacity, $\lambda_{\text{eff.}}$ is the effective thermal conductivity, $\bar{\tau}_{ij}$ is the stress tensor of the mean flow, τ_{ij}^R is the Reynolds stress tensor and u_i is the velocity vector. The terms in red represent different routes for the conversion of mean flow kinetic energy into enthalpy through pressure work and molecular & turbulent viscous shear work (*i.e.,* viscous dissipation). The term in blue $\dot{\omega}_T$ is the endothermic heat sink rate and is defined as

$$\dot{\omega}_T \approx \sum_{k=1}^{N_{\text{spe.}}} \Delta h_{f,k}^0 \cdot \dot{\omega}_k \tag{3}$$

where $\dot{\omega}_k$ are the net species production rates and $\Delta h_{f,k}^0$ the standard formation enthalpies.

Crucially, from Eq. (2), it can be seen that to maintain a constant idealized reaction temperature level, $\frac{D\bar{T}}{Dt} = \frac{\partial\bar{T}}{\partial x_j} = 0$, subject to temperature sinks due to the endothermic reaction, the combination of pressure work and viscous dissipation must be designed to approximately balance the endothermic sink term $\dot{\omega}_T$ at each streamwise location, as illustrated in Fig. 7.

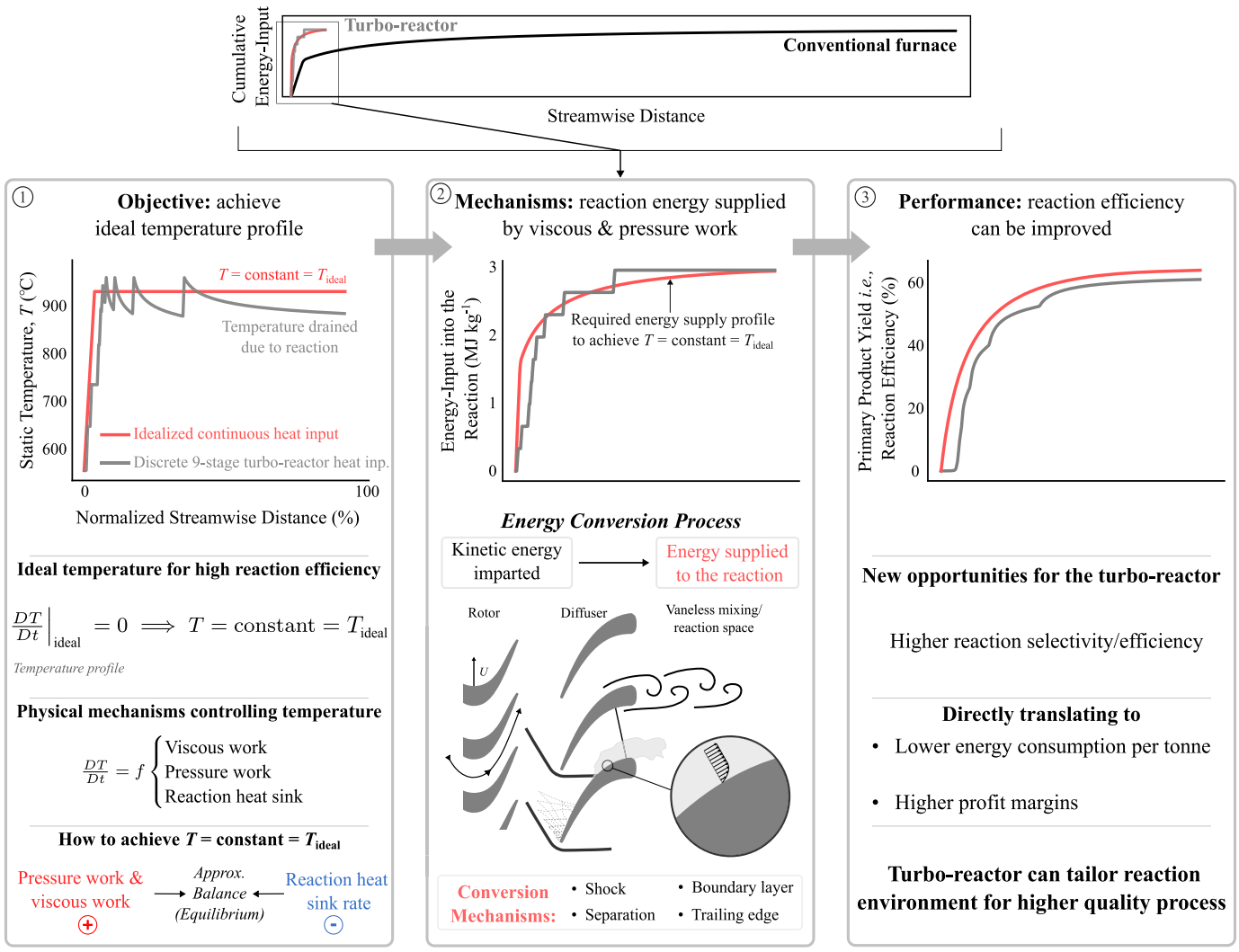

Fig. 7. Designing a reaction efficient temperature profile along the turbo-reactor bladed flow path.

3.1.2. Box ②: Energy conversion mechanisms

The aerodynamic designer is trying to shape the turbo-reactor flow path to achieve an energy supply profile to the reaction such that an ideal reaction-efficient temperature profile is matched. Box ② in Fig. 7 shows the energy conversion profile required to maintain some idealized temperature profile shown in Box ①. Through a series of discrete stages, the turbo-reactor attempts to approximate it.

There are reversible (isentropic) and irreversible (entropic) mechanisms responsible for this energy conversion profile. The first term in red in Eq. (2) is the reversible pressure work $\overline{u}_i \frac{\partial \bar{p}}{\partial x_i}$. This is a consequence of changes in the flow area and the reversible pressure rise component of the shock action.

The remaining energy conversion is provided by irreversible (entropic) energy conversion mechanisms through viscous shear work. These are accounted for by $(\bar{\tau}_{ij} + \tau^R_{ij}) \frac{\partial \bar{u}_i}{\partial x_j}$ in Eq. (2). Some of the primary physical mechanisms are highlighted at the bottom of Box ② in Fig. 7.

3.1.3. Box ③: Reaction performance

Controlling the balance between the endothermic sink and the dissipation profile at each streamwise location to better match an ideal reaction-efficient temperature profile can lead to improved reaction efficiency, as illustrated in box ③ of Fig. 7. To understand the importance of improving the reaction efficiency (*i.e.,* the yields), it is highlighted that for a typical hydrocarbon cracking plant (with capacity equal to 1 million tonnes of feed per year), a 10% improvement in reaction efficiency can increase annual profits by €60 – €90 million (as of 2024). This underscores the importance of tailoring the aerothermal design for improved yields. Note that this figure is calculated assuming a typical naphtha feedstock cost between 600 and 900 euros per tonne of feedstock [15].

It should be noted that the approach of striving for a *constant* ideal reaction temperature is not necessarily the current design strategy nor is it optimal for a general chemical reaction. However, it is a useful way to think about design goals: balancing viscous dissipation and reaction heat sink to produce a reaction-efficient temperature profile (see Fig. 7). For different feedstocks or reactions, the ideal temperature level may vary and/or may not be constant, leading to a nonequilibrium balance where $\frac{D\bar{T}}{Dt} \neq 0$.

3.2. Theoretical limit on the rate of energy conversion

To understand the potential range of temperature profile control, it is useful to determine the idealized energy conversion rate limit. This is set using a single normal shockwave with a high preshock Mach number (M_{preshock}), as shown in Fig. 8. The idealized energy conversion profile in Fig. 8 is determined from 1-D compressible flow equations with inlet properties determined from a meanline calculation. The supersonic flow is isentropically expanded (see Fig. 8) to a Mach number such that when it is terminated by a shock, the gas pressure is

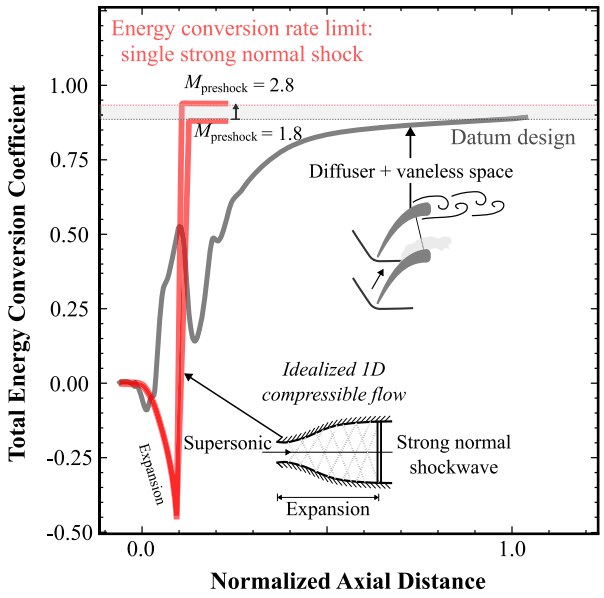

Fig. 8. A comparison of the total energy conversion coefficient (Eq. (6)) achieved with the datum design against the idealized limit transferable through a single normal shockwave within a 1-D nozzle.

raised to the fixed backpressure. It can be seen that over just a few millimeters, a single shock can dissipate over 90% of the incoming kinetic energy. However, the shock action yields diminishing returns with increasing M_{preshock}.

For rapidly preheating the gas mixture before the reaction phase, further capitalizing on shock action (see Fig. 8) could be a useful technique to reduce the flow path length by increasing the rate of energy conversion. However, in the reaction zone, which demands a specific temperature profile for maximum reaction efficiency, such a rapid rate of energy conversion may not be ideal for the reaction.

3.3. Defining energy conversion metrics

In conventional design practice, loss coefficients are used to quantify efficiency penalties and facilitate blade design comparisons. For the turbo-reactor design, the goal is to quantify the amount of incoming kinetic energy that is converted into enthalpy of the reaction. To quantify the irreversible (entropic) component of energy conversion, the relevant metric is the enthalpy loss coefficient used for conventional machines, as described by Denton [3]. However, in this case, we call it the "irreversible energy conversion coefficient". This coefficient is defined for a perfect gas as follows:

$$\zeta_{h,s} = \frac{c_p(T_{\text{exit}} - T_{\text{isentropic}})}{0.5V_1^2} \tag{4}$$

where subscript "1" defines the diffuser inlet and subscript "exit" defines the end of the vaneless space (see Fig. 9). The value of $T_{\text{isentropic}}$ is the static temperature obtained in an isentropic compression process that ends at the same final pressure as the actual process. By definition, the total energy conversion coefficient is defined as

$$\zeta_h = \zeta_{h,s} + \zeta_{h,\text{rev.}} = \frac{c_p(T_{\text{exit}} - T_1)}{0.5V_1^2}. \tag{5}$$

This represents the total change in enthalpy of the working fluid across the diffuser normalized by the incoming kinetic energy of the flow. By subtracting the irreversible energy conversion coefficient (Eq. (4)) from the total (Eq. (5)), the reversible (isentropic) component of the conversion coefficient must be defined as

$$\zeta_{h,\text{rev.}} = \frac{c_p(T_{\text{isentropic}} - T_1)}{0.5V_1^2} \tag{6}$$

4. Numerical methodology

A combination of unsteady Reynolds-averaged Navier–Stokes (URANS) and high-fidelity large-eddy simulation (LES) strategies has been used to illustrate the mechanisms responsible for the energy conversion process along the flow path. The following section (Section 4.1) describes the methodology developed to decompose the flowfield into the various mechanisms.

4.1. Energy conversion budget domain decomposition

Metrics

To decompose the energy conversion process into its constituent irreversible mechanisms, as shown in Fig. 9, a similar approach is taken to that of Pullan et al. [16] and Zhao et al. [17]. The domain is zonally decomposed into 11 spatial subvolumes intimately linked to the physical mechanisms discussed in Section 3.1. The Favre-averaged viscous dissipation rate (see Eq. (2)) is volume-integrated over each subvolume:

$$\Phi_\tau = \frac{\iiint_{\mathcal{V}} (\bar{\tau}_{ij} + \tau_{ij}^R) \frac{\partial \tilde{u}_i}{\partial x_j} d\mathcal{V}}{0.5\dot{m}V_1^2} \tag{7}$$

where $\mathcal{V}$ is the subvolume integrated over, $\dot{m}$ is the mass flow rate and V_1 is the diffuser inlet velocity. To quantify the reversible share of energy conversion, the pressure work term in Eq. (2) must also be volume-integrated:

$$\Phi_p = \frac{\iiint_{\mathcal{V}} \bar{u}_i \frac{\partial \bar{p}}{\partial x_i} d\mathcal{V}}{0.5\dot{m}V_1^2} \tag{8}$$

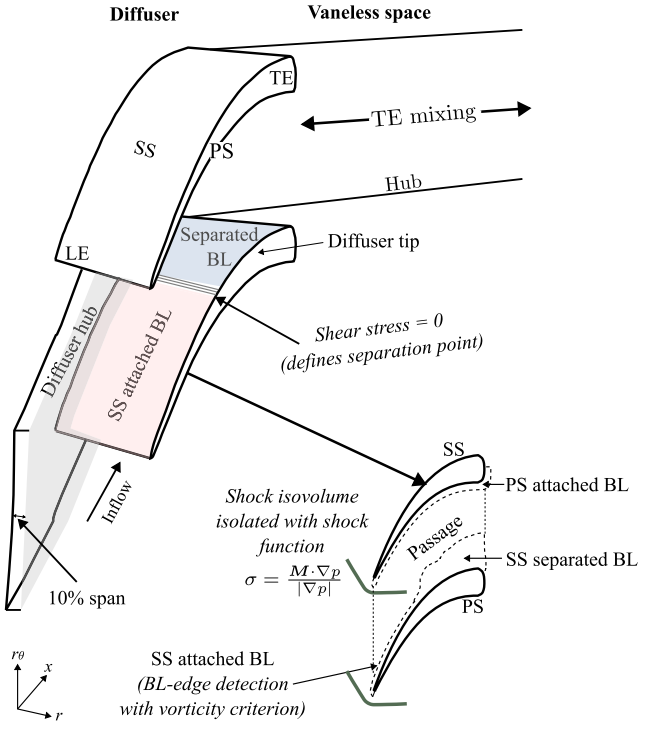

Fig. 9. A schematic illustrating the domain decomposition for the energy conversion breakdown analysis.

In conventional loss analysis, the term used to identify a source of loss is the entropy generation rate [3,18]. However, in the turbo-reactor, since the main objective of the energy conversion breakdown analysis is to identify sources that contribute to the conversion of kinetic energy into energy available for the reaction, the most relevant transport equation is the enthalpy (see Eq. (2)) rather than the entropy transport equation. Therefore, Eq. (2) implies that the viscous dissipation rate is the most appropriate metric.

Shock capturing

The isovolumes associated with a shockwave (see blue isovolumes at the Top of Fig. 12(*a*)) are identified using a criterion based on the shock function [19]:

$$\sigma = \frac{\boldsymbol{M} \cdot \nabla p}{|\nabla p|} \tag{9}$$

where $\boldsymbol{M}$ is the Mach number vector.

Boundary layer decomposition

The proceeding analysis distinguishes between an attached and a separated boundary layer. The boundary layer (BL) separation point is defined as the point where the wall shear stress falls to zero (see Fig. 9). The attached boundary layer edge at each streamwise location is determined as the pitchwise station with minimum radial vorticity.

Endwalls

The endwall flow at hub and tip is assumed to be all of the flow within 10% of the respective endwall. This includes the corner flow between the endwalls and the blade surfaces. Tip leakage is not included in this analysis.

Passage freestream mixing

The remaining mesh cells not yet classified are associated with passage freestream mixing.

Trailing edge mixing

In the vaneless space, all the non-endwall mesh cells immediately downstream of the diffuser trailing edge (TE) are associated with "TE mixing" (see Fig. 9).

4.2. Numerical setup

The in-house computational fluid dynamics solver Tblock [20,21] is used for all numerical investigations. The ability of Tblock to accurately predict the flowfield where the Reynolds number is similar to that observed in the turbo-reactor has been validated by Rosic et al. [22]. All numerical simulations are performed without a reaction model, and the working fluid is modeled as a calorically perfect gas. This assumption is reasonable since only a single stage is studied and thus the thermophysical fluid properties do not change significantly within this truncated domain. Furthermore, the density changes induced by the reaction are not large enough to have a noticeable effect on the energy conversion breakdown within a single stage. Therefore, neglecting aerochemical interactions is a suitable approach for this analysis.

LES: Full stage

The full-stage wall-modeled LES domain contains $226 \times 152 \times 152$ nodes in the axial, spanwise and pitchwise directions within the blade passages (totaling 120 million grid points across the whole domain), leading to an average $y^+ = 4.1$ in the diffuser–vaneless-space system. The Smagorinsky subgrid-scale model with van Driest damping is employed. For fixed Mach number M and Reynolds number Re computations, it can be assumed that $Re = 700,000$ and $M = 1.2$, in which $Re = \frac{\rho_1 V_1 b_{\text{true}}}{\mu}$ based on the diffuser inlet conditions, $\rho_1 V_1$, and the true chord length is b_{true} and μ is the molecular viscosity.

Table 1
URANS mesh sensitivity for the entropy loss coefficient ζ_s and the irreversible $\zeta_{h,s}$ & total ζ_h energy conversion coefficients.

Blade passage grid sizes	ζ_s	$\zeta_{h,s}$	ζ_h
$122 \times 81 \times 81$	0.67	0.63	0.90
$153 \times 103 \times 103^*$	0.65	0.63	0.89
$183 \times 123 \times 123$	0.65	0.63	0.89

URANS: Diffuser and vaneless space domain

For parametric studies on the influence of the Reynolds and Mach number on the energy conversion breakdown, a truncated domain with only diffuser and vaneless space has been used (see Fig. 9).

The inlet boundary condition is taken as the 2-D nonuniform time-averaged field from an unsteady full-stage calculation. From precursor numerical computations, it was found that periodic unsteadiness from the passing of the upstream rotor wakes has only a minimal impact on the energy conversion breakdown. This implies that the dissipation mechanisms respond linearly to wake-induced perturbations in diffuser inlet conditions. Therefore, the diffuser can be safely isolated for this analysis. This is useful because it allows the direct influence of Reynolds and Mach numbers on energy conversion to be decoupled from variations in the upstream flowfield entering the diffuser due to changes in the operating regime.

The following approach is used to vary the Mach number and Reynolds number independently. The Reynolds number can be set by varying the molecular viscosity to match the desired Reynolds number. The Mach number can be set by varying the isobaric heat capacity for a fixed ratio of specific heats.

Table 1 indicates sufficient mesh independence with a domain of $153 \times 103 \times 103$ grid points in the axial, spanwise and pitchwise directions (totaling 18 million grid points), producing an average $y^+ = 5.4$ at the design point. The Spalart–Allmaras turbulence model is employed with wall functions. Due to a high turbulence intensity [4], fully turbulent boundary layers are used. Fig. 10 shows a comparison of a URANS and LES computation. The URANS calculation shows good agreement with high-fidelity LES, which provides confidence in the numerical results presented.

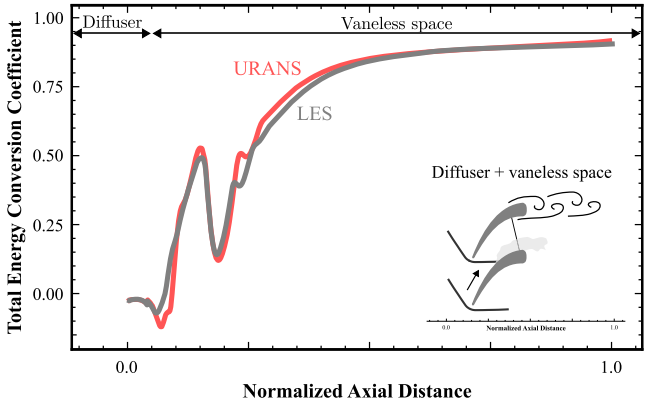

Fig. 10. A comparison of LES and URANS computations for the total energy conversion coefficient, ζ_h (see Eq. (5)) across the diffuser–vaneless-space system.

5. Energy conversion mechanisms

To enable fine-tuning of the energy conversion profile, it is important to understand the energy transformation processing mechanisms. This will inform future aerothermochemical design optimization to better match the optimal temperature profile for the chemistry (see Section 3.1). For example, the diffuser blade profile could be modified and/or the vaneless space length can be varied stage by stage (see Figs. 4 & 5).

5.1. Aerodynamically-tuned: Energy transfer process

Before the energy conversion process is illustrated in detail using numerical simulations, it is instructive to see how the aerodynamic losses (*i.e.,* the entropy rise) vary across the stator–rotor system (where mechanical energy is imparted). Fig. 11 highlights a clear distinction between the stator–rotor system and diffuser–vaneless-space system. While the latter is designed to amplify losses to chemically tune the reaction, the former is aerodynamically tuned, which is more in accordance with conventional turbomachinery design practice. However, while conventional design focuses on increasing efficiency across the rotor and throughflow capacity per unit frontal area of the machine, the design of the turbo-reactor stator–rotor system is more concerned with developing a high work coefficient as well as throughflow capacity. This directly translates into reducing flow deviation and blockage, which, of course, is strongly correlated with reducing the entropy rise (see Fig. 11). However, it is not necessarily the absolute minimum entropy rise that corresponds to the maximum power input.

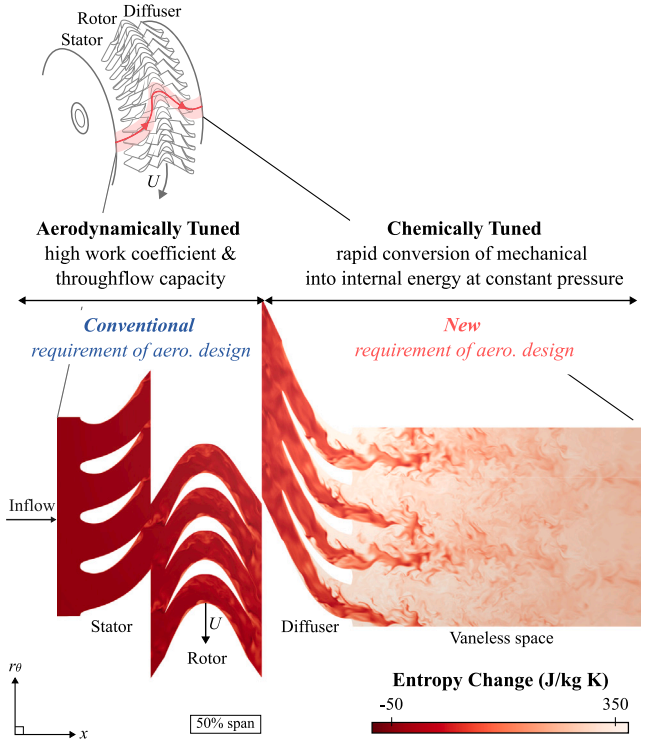

Fig. 11. Single stage instantaneous entropy change (LES).

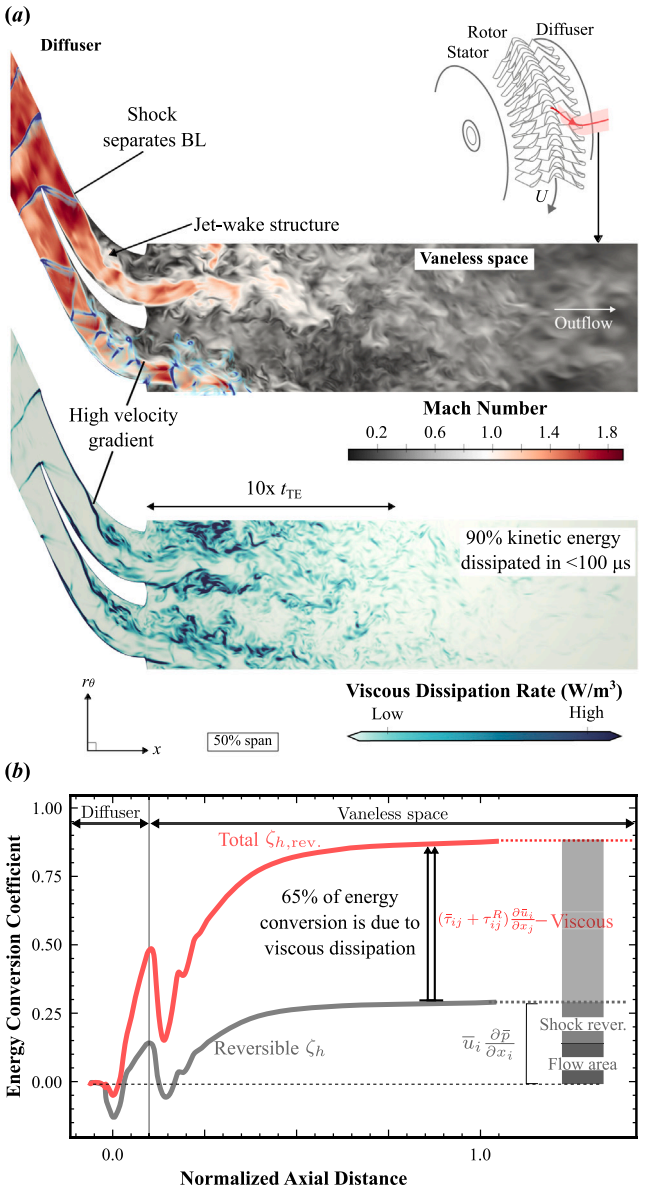

Fig. 12. (*a*) Instantaneous Mach number with superimposed numerical schlieren in blue (first) and viscous dissipation (second), and (*b*) time- and mass-averaged total (ζ_h) and reversible ($\zeta_{h,\mathrm{rev.}}$) energy conversion coefficient (LES).

5.2. Chemically-tuned: Energy conversion process

Fig. 12(*a*) shows the energy conversion process in the diffuser–vaneless system. Irreversibilities dominate over reversible pressure work, accounting for a 65% share (see Fig. 12(*b*)). This is primarily a consequence of turbulent rather than molecular viscosity. The diffuser blade row accounts for 55% of the total energy conversion. Within 10× diffuser TE thicknesses (t_{TE}), the energy conversion process is almost complete and, strikingly, ~90% ($\zeta_h \approx 0.9$) of the incoming kinetic energy is dissipated in under 100 µs (see Fig. 12(*b*)). The loss coefficient is approximately 10 times that developed in a compressor. Uniform conditions are quickly established just downstream of the diffuser TE, which is crucial for optimal reaction performance.

The remaining 35% of energy conversion is composed of fairly equal contributions from the reversible pressure gain component of the shock-induced temperature rise and isentropic diffusion of the flow (see Fig. 12(*b*)). Energy conversion across the thin shock layer has two distinct contributions (see Eq. (2)).

(1) Reversible pressure work (accounted for by $\overline{u}_i \frac{\partial \bar{p}}{\partial x_i}$).

(2) Irreversibilities (accounted for by $(\bar{\tau}_{ij} + \tau^R_{ij})\frac{\partial \bar{u}_i}{\partial x_j}$).

At low Mach numbers (M), the former dominates, but as M increases, the latter begins to dominate [23]. It will be shown in Section 5.3 that the temperature change due to entropy produced in the shock system is almost negligible. Therefore, the overall contribution of the shock system is about 20% (see Fig. 12(*b*)), primarily due to reversible pressure work rather than entropy rise.

Fig. 12(*a*) suggests that the dominant impact of the shock system on the irreversible energy conversion rate is an indirect rather than direct effect. The indirect impact of the shock system is the result of shockwave boundary layer interaction (SWBLI). Shock impingement separates the suction surface (SS) boundary layer at approximately 50% of the chord. The high-entropy boundary layer unravels and spreads, mixing out the hot boundary layer fluid into the freestream. At the

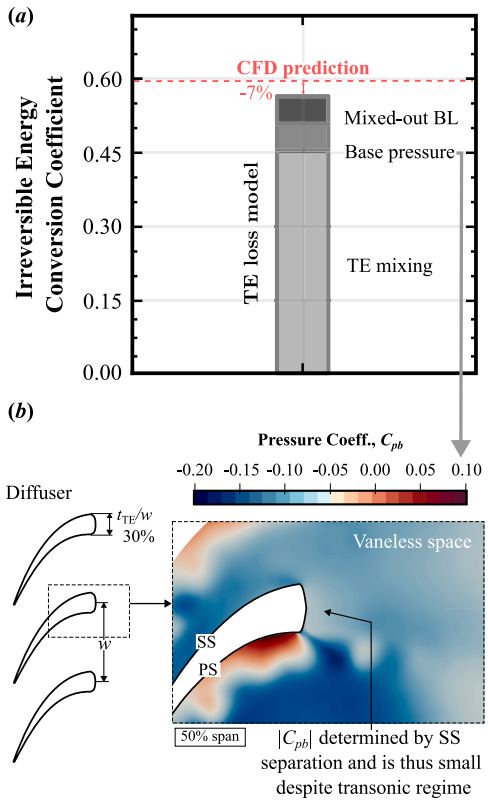

Fig. 13. (*a*) Irreversible energy conversion coefficient predicted by a modified Denton TE loss model [3,25] and (*b*) time-averaged pressure coefficient ($C_{pb} = \frac{p-p_{ref}}{p_{01}-p_{ref}}$, where p_{ref} is the average pressure PS and SS before the TE circle).

interface between the separated backflow region and the freestream jet above it, a large velocity gradient is generated (see Fig. 12(*a*)). This leads to intense deformation shear work ($(\bar{\tau}_{ij} + \tau^R_{ij})\frac{\partial \bar{u}_i}{\partial x_j}$) at the interface (see Fig. 12(*a*)). Furthermore, Fig. 12(*a*) (Top) shows, in blue, the footprint of a shock diamond within the overexpanded jet that exits the diffuser passage. This has important implications for TE mixing [24].

Despite the transonic flow regime and the thick TE occupying $t_{TE}/w \approx 30\%$ of the blade pitch w, surprisingly, Fig. 13 implies a minimal impact of the base pressure coefficient C_{pb} on TE loss. It is calculated as $C_{pb} \approx -0.05$ around the TE circle, which is several times smaller in magnitude than that of a transonic turbine ($C_{pb} \approx -0.3$) [24]. This is because, despite the global transonic flow regime, the flow locally around the TE circle is in the low subsonic regime and the pressure level is set by the SS separation (see Fig. 13(*b*)). Therefore, the magnitude of the base pressure is low, in the range experienced by subsonic blading.

Downstream, most of the mechanical energy dissipation is due to the mixing of two bulk streams — the jet and the separated wake (see Fig. 12(*a*)) — which have widely different stagnation pressures. The entropy generated in velocity equilibration to restore uniform flow is directly related to the difference in stagnation pressures between the jet and the wake [3]. Since this is large (see Fig. 12(*a*)), the downstream mixing intensifies. To model this mixing with a reduced-order model, a modified version of Denton's TE loss model [3,25] shown in Fig. 13(*a*) provides a fairly accurate estimate of the energy conversion despite the model being extrapolated substantially beyond its typical application range. Remarkably, the irreversible energy conversion coefficient is only underestimated by 7%.

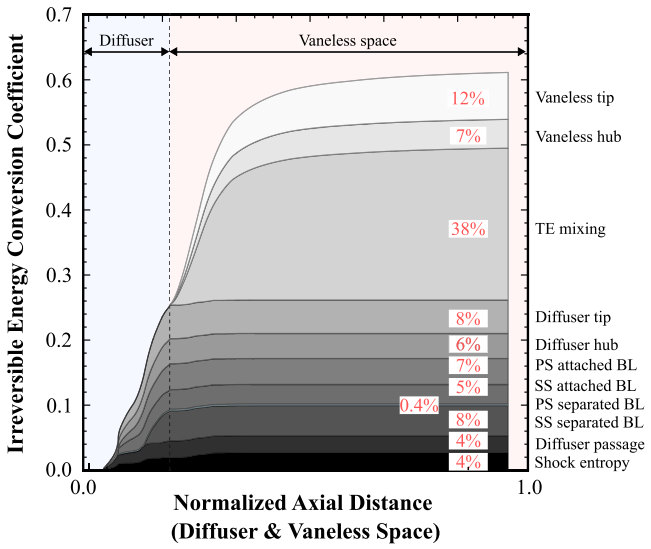

Fig. 14. Streamwise evolution of the irreversible energy conversion coefficient breakdown.

5.3. Global energy conversion breakdown analysis

Based on the domain decomposition introduced in Section 4.1, Fig. 14 shows the streamwise evolution of the irreversible energy conversion breakdown for a typical design and boundary conditions. Most importantly, it is clear that turbulent dissipation generated downstream of the diffuser TE is the dominant mechanism, accounting for 38% of the irreversible total. This process quickly reaches its maximum proportion within $1C_x$ (see Fig. 14). Because the SS boundary layer separates far upstream of the TE (see Fig. 12(*a*)), such a thick TE may not be necessary to encourage intense mixing (although it is beneficial from a thermomechanical perspective). However, in general, the TE thickness sets the turbulent length scale and the energy conversion rate scales with its thickness.

There are three further conclusions to be drawn from Fig. 14. First, the pressure-surface (PS) attached boundary layer energy conversion dominates over the SS BL because it remains attached longer. The SS boundary layer separates earlier (see Fig. 12(*a*)) and is therefore the most significant contribution within the diffuser passage. Second, in both the diffuser passage and vaneless space, the tip flow near the endwall generates more entropy than at the hub because the Mach number is higher and more mass flow is concentrated (which is implied by radial equilibrium). Finally, the viscous dissipation within the shock system is relatively small, as it mainly comprises relatively weak oblique shocks. This is consistent with the fact that the entropy change across a shock is only of third order in shock strength.

5.4. Mach and Reynolds number effects

For a perfect gas, three nondimensional flow parameters govern the energy conversion process in the diffuser: the Reynolds number, Mach number and diffuser inlet flow angle. This section explores Reynolds and Mach number effects over an engine-relevant range using four samples to cover each nondimensional group. This representative range covers the variability of nondimensional groups across the multistage environment [7]. Due to the unique incidence condition [26], the inlet flow angle is not constant as the diffuser inlet Mach number varies; however, it only varies by ~1°.

As the diffuser inlet Mach number increases for a fixed Reynolds number (Re = 700,000), Fig. 15 shows that the irreversible component of the energy conversion coefficient decreases while the reversible component increases. The reversible component increases with Mach

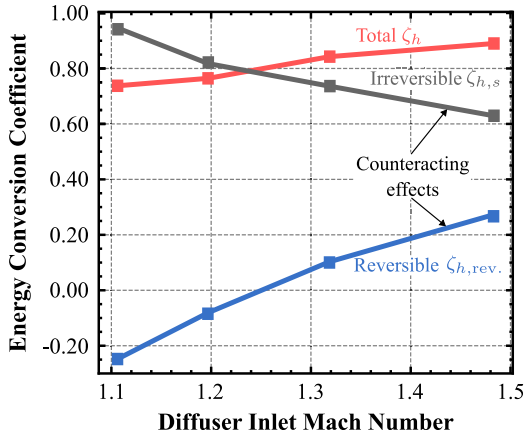

Fig. 15. Energy conversion coefficients as a function of diffuser inlet Mach number for a fixed Reynolds number.

number for two reasons. First, there is a greater contribution of the reversible pressure work through the shock system (see Fig. 15) due to an increased pressure ratio. Second, the passage isentropic flow diffusion increases due to changes in the effective flow area.

As a result of the counteracting dependence of the reversible and irreversible energy conversion coefficient with the Mach number, the change in the total energy conversion coefficient is weaker than expected with only a 20% increase in ζ_h within the range $1.1 \leq M \leq 1.5$. However, this effect should still be taken into account when designing a multistage machine in which the Mach number decreases towards the rear. This will influence the design of the reaction-efficient temperature profile.

Fig. 16(*a*) indicates that although the overall distribution of irreversible energy conversion mechanisms does not change dramatically, its overall magnitude decreases by 33% with increasing Mach number. A key factor is the reduction in normalized dissipation in the attached blade and endwall boundary layers. This is likely to be a consequence of two factors. First, the dissipation coefficient C_d is known to decrease with Mach number (for a fixed Reynolds number) [27], but only marginally. Second, it was found that at higher Mach numbers, the flow acceleration in the passage is reduced, changing the state of the boundary layer and leading to a lower C_d. Furthermore, the diffuser exit flow angle α was found to decrease by 13° over the range. This directly translates to lower TE mixing ($\zeta_{h,s} \propto 1/(w \cos \alpha)$), as seen in Fig. 16(*a*), as a result of reduced sudden flow expansion.

Compared to the Mach number, the consequence of Reynolds number variability is negligible and the energy conversion breakdown is approximately independent of the Reynolds number over a range from 0.4 to 1.4 million, as shown in Fig. 16(*b*). The Mach number is fixed at $M = 1.2$. There is a minor drop in the irreversible energy conversion coefficient at higher Reynolds numbers, since dissipation is inversely related to Re. Reynolds number independence is perhaps expected, since Re is above the critical Reynolds number ($Re_{\mathrm{crit}} \approx 100,000$) and turbulence intensity at the diffuser inlet is high (≥10%).

5.5. Compact multistage architecture

So far, the domain investigated has been a single stage with an extended vaneless space, which is required by the reaction. For preheating the nonreacting feedstock mixture before reaction activation, temperature profiling is unnecessary and a "compact" turbo-reactor

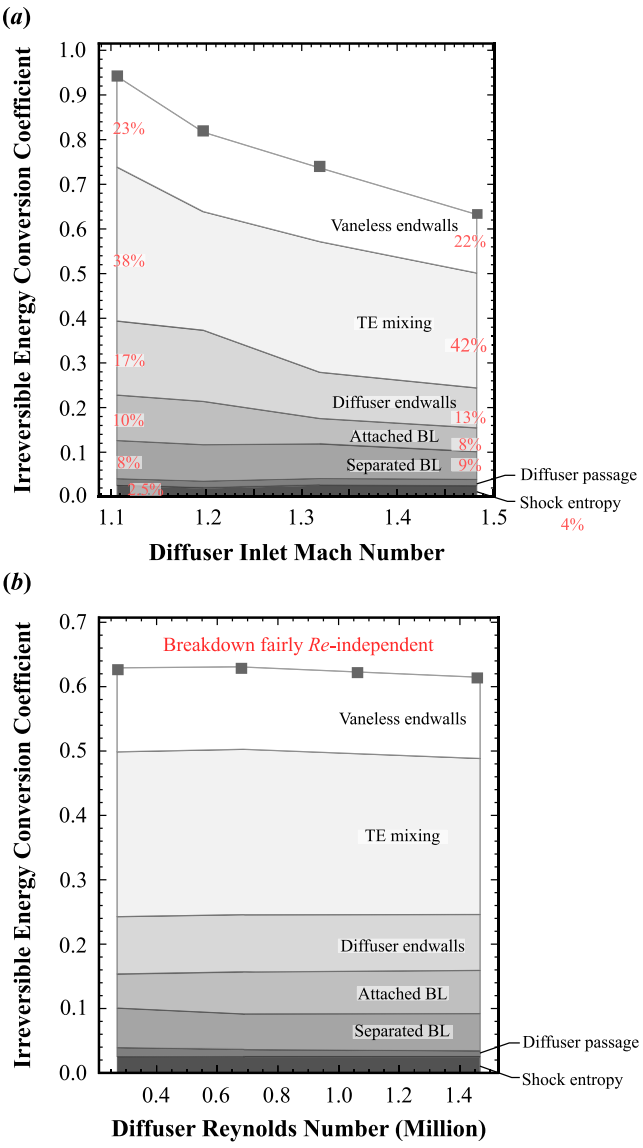

Fig. 16. The irreversible energy conversion coefficient as a function of: (*a*) diffuser inlet Mach number and (*b*) Reynolds number, $Re = \frac{\rho_1 V_1 b_{\mathrm{true}}}{\mu}$, based on the diffuser inlet conditions, $\rho_1 V_1$, and its true chord length, b_{true}.

stage can be adopted (see Fig. 4). Since the vaneless mixing space is absent, the flow can maintain a higher Mach number when it enters stages 2 to 4 relative to the first stage.

Fig. 17 illustrates that despite the removal of the vaneless mixing space by integrating stator and diffuser, it is still possible to dissipate a large amount of mechanical energy within each stage, albeit through different mechanisms. Whereas previously TE mixing dominated, now it no longer plays a significant role in the energy conversion process prior to the final diffuser. Instead, viscous dissipation within the blade surface and endwall boundary layers dominates. This is driven by an increasing freestream velocity across the multistage environment. Energy conversion near the endwalls is high as a result of additional strong secondary flows present here.

6. Summary and conclusions

This paper has explained that the turbo-reactor can be designed as a "chemically tuned" device in which the bladed path is tailored to optimize the reaction dynamics of a given feed. For the first time in

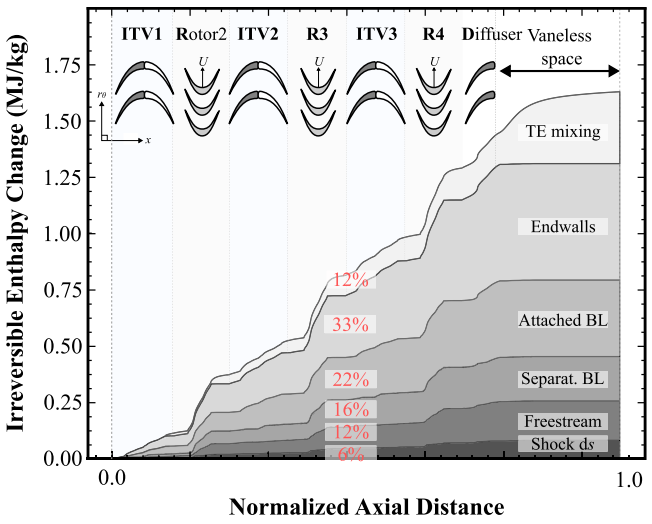

Fig. 17. Streamwise breakdown of the irreversible component of enthalpy change across the multistage compact turbo-reactor architecture.

turbomachinery, aerodynamic losses can be leveraged to control the rate of energy conversion into the reaction and thus design a reaction-efficient temperature profile. This can be achieved by optimally balancing dissipation against the endothermic sink term. By introducing new vectors of energy quality for turbomachines, that is, chemical exergy and reaction efficiency, the thermodynamic implications of converting electricity to heat have been clarified.

To enable optimization of the aerodynamic design to better match the ideal energy supply profile into the chemical reaction, it is crucial to explore the mechanisms responsible for the energy conversion process. A series of numerical investigations have been performed to examine the breakdown of energy conversion mechanisms. Several conclusions have been drawn.

(1) Irreversible energy conversion overshadows reversible pressure rise contributions, accounting for 65%. Of this 65%, turbulent viscous dissipation downstream of the diffuser trailing edge (TE) is the dominant entropic mechanism (at 25% of the total). This is also a critical process for rapidly homogenizing the reaction for improved performance.

(2) The total contribution of the shock system was around 20%, mainly due to a reversible pressure work mechanism rather than entropy rise. The dominant irreversible contribution of the shock system is an indirect one through shockwave boundary layer interaction. This process separates the boundary layer early in the passage and initiates a strong mixing process that continues downstream of the trailing edge.

(3) The energy conversion breakdown has been explored over a range of Mach and Reynolds numbers. Over a wide range of flow regimes it is possible to dissipate a large fraction of the incoming kinetic energy (≥60%). The energy conversion coefficient was independent of Reynolds number within a realistic range. As expected, the Mach number had a more significant influence. However, due to counteracting effects from reversible and irreversible energy conversion, the effect was relatively weak with only a 20% increase in the total energy conversion coefficient with Mach number rising from 1.1 to 1.5.

(4) For the compact stage design, the energy conversion rate remains high despite eliminating the interstage vaneless mixing space. This is partly a consequence of elevated skin friction due to increased flow speeds.

For the analysis presented, tip leakage was intentionally neglected. This is representative of a shrouded stationary blade row. However, a future study can incorporate leakages if necessary.

We hope that this paper can help to open an entirely new field of research into tuning the aerothermal design of turbomachines to control and optimize chemical transformations along the bladed flow path through careful temperature profile design.

Declaration of competing interest

The authors declare that they have no known competing financial interests or personal relationships that could have appeared to influence the work reported in this paper.

Acknowledgments

Dylan Rubini was supported by funding from the Engineering and Physical Sciences Research Council (Grant number 2441788). The authors thank N. Karefyllidis for providing the stage dataset. The authors appreciate the fruitful discussions with N. A. Cumpsty. The computational resources used were provided by ARCHER2.

Appendix. Exergy

Total specific exergy is defined as follows:

$$b_{\mathrm{ex}}^{tot} = b_{\mathrm{ex}}^{Tp} + b_{\mathrm{ex}}^{ch} \tag{10}$$

The physical (thermomechanical) component of the total exergy is:

$$b_{\mathrm{ex}}^{Tp} = (h_0 - h_{0,\mathrm{ref}}) - T_{\mathrm{ref}}(s - s_{\mathrm{ref}}) \tag{11}$$

where the subscript $\square_{\mathrm{ref}}$ is the thermochemical state of the reference environment [28], h_0 is the stagnation enthalpy and s is the entropy. The chemical exergy is:

$$b_{\mathrm{ex}}^{ch} = \sum_{k=1}^{N_{\mathrm{spe.}}} Y_k b_{\mathrm{ex},k}^{ch,ref} + RT_{\mathrm{ref}} \sum_{k=1}^{N_{\mathrm{spe.}}} X_k \ln X_k \tag{12}$$

where X_k are the species mole fraction, Y_k are the mass fractions, and $b_{\mathrm{ex},k}^{ch,ref}$ is the chemical exergy of each species.

Chemical exergy is the result of the chemical disequilibrium of a species with the reference environment. This is calculated using the Gibbs function defined for a chemical reaction between the substance in question and the reference environment. In theory, useful work can be obtained from a chemical resource (species) by promoting a reaction until a chemical equilibrium is reached with the reference environment. The chemical exergy $b_{\mathrm{ex},k}^{ch,ref}$ of various chemical species, fuels and materials can be found tabulated by Szargut et al. [28]. Calculating the chemical exergy of species is also discussed in Michalakakis et al. [29]. Note that for most hydrocarbon fuels, the chemical exergy is very similar to the heating value of the fuel.

Data availability

The data that has been used is confidential.

References

[1] J.H. Horlock, Advanced gas turbine cycles: a brief review of power generation thermodynamics, 2013.
[2] E. Michaelides, Exergy Analysis for Energy Conversion Systems, Cambridge University Press, 2021.
[3] J.D. Denton, The 1993 IGTI scholar lecture: Loss mechanisms in turbomachines, ASME J. Turbomach. 115 (4) (1993) 621–656, https://doi.org/10.1115/1.2929299, 10.
[4] D. Rubini, L. Xu, B. Rosic, H. Johannesdahl, A new turbomachine for clean and sustainable hydrocarbon cracking, ASME J. Eng. Gas Turbines Power 144 (2) (2021) 021024, https://doi.org/10.1115/1.4052784, 12.

[5] D. Rubini, N. Karefyllidis, L. Xu, B. Rosic, H. Johannesdahl, A new robust regenerative turbo-reactor concept for clean hydrocarbon cracking, J. Glob. Power Propuls. Soc. 6 (2022) 135–150, https://doi.org/10.33737/jgpps/150550.
[6] N. Karefyllidis, D. Rubini, B. Rosic, L. Xu, V.-M. Purola, A novel axial energy-imparting turbomachine for high-enthalpy gas heating: Robustness of the aerodynamic design, ASME J. Turbomach. 146 (3) (2023) 031005, https://doi.org/10.1115/1.4063928, 11.
[7] D. Rubini, N. Karefyllidis, B. Rosic, L. Xu, E. Nauha, Decarbonisation of high-temperature endothermic chemical reaction processes using a novel turbomachine: Robustness of the concept to feed variability, J. Glob. Power Propuls. Soc. 8 (2024) 111–126, http://dx.doi.org/10.33737/jgpps/185623.
[8] R. Chauhan, R. Sartape, N. Minocha, I. Goyal, M.R. Singh, Advancements in environmentally sustainable technologies for ethylene production, Energy Fuels 37 (17) (2023) 12589–12622, http://dx.doi.org/10.1021/acs.energyfuels.3c01777.
[9] O. Mynko, M. Bonheure, I. Amghizar, D.J. Brown, L. Chen, G.B. Marin, R. Freitas de Alvarenga, D. Civancik Uslu, J. Dewulf, K.M. Van Geem, Electrification of steam cracking as a pathway to reduce the impact of the petrochemical industry on climate change, J. Clean. Prod. 427 (2023) 139208, http://dx.doi.org/10.1016/j.jclepro.2023.139208.
[10] G.P. Thiel, A.K. Stark, To decarbonize industry, we must decarbonize heat, Joule 5 (3) (2021) 531–550, http://dx.doi.org/10.1016/j.joule.2020.12.007.
[11] M.E.H. Tijani, H. Zondag, Y. Van Delft, Review of electric cracking of hydrocarbons, ACS Sustain. Chem. Eng. 10 (49) (2022) 16070–16089, https://doi.org/10.1021/acssuschemeng.2c03427.
[12] T. Dickens, I. Day, The design of highly loaded axial compressors, ASME J. Turbomach. 133 (3) (2010) 031007, https://doi.org/10.1115/1.4001226, 11.
[13] M. Ghashghaee, R. Karimzadeh, Multivariable optimization of thermal cracking severity, Chem. Eng. Res. Des. 89 (7) (2011) 1067–1077, http://dx.doi.org/10.1016/j.cherd.2010.12.002.
[14] T. Poinsot, D. Veynante, Theoretical and Numerical Combustion, RT Edwards, Inc., 2005.
[15] IEA, Simplified Levelised Cost of Petrochemicals for Selected Feedstocks and Regions, IEA, Paris, France, 2017, https://www.iea.org/data-and-statistics/charts/simplified-levelised-cost-of-petrochemicals-for-selected-feedstocks-and-regions-2017.
[16] G. Pullan, J. Denton, E. Curtis, Improving the performance of a turbine with low aspect ratio stators by aft-loading, ASME J. Turbomach. 128 (3) (2004) 492–499, https://doi.org/10.1115/1.2182000, 03.
[17] Y. Zhao, R.D. Sandberg, Using a new entropy loss analysis to assess the accuracy of RANS predictions of an high-pressure turbine vane, ASME J. Turbomach. 142 (8) (2020) 081008, https://doi.org/10.1115/1.4046531, 07.
[18] M.B. Zlatinov, C. Sooi Tan, M. Montgomery, T. Islam, M. Harris, Turbine hub and shroud sealing flow loss mechanisms, ASME J. Turbomach. 134 (6) (2012) 061027, https://doi.org/10.1115/1.4006294, 09.
[19] D. Lovely, R. Haimes, Shock detection from computational fluid dynamics results, in: 14th Computational Fluid Dynamics Conference, 1999, p. 3285, https://doi.org/10.2514/6.1999-3285.
[20] J.D. Denton, An improved time-marching method for turbomachinery flow calculation, ASME J. Eng. Gas Turbines Power 105 (3) (1983) 514–521, https://doi.org/10.1115/1.3227444, 07.
[21] J.D. Denton, The use of a distributed body force to simulate viscous effects in 3D flow calculations, in: Volume 1: Turbomachinery, Turbo Expo: Power for Land, Sea, and Air, Vol. Volume 1: Turbomachinery, 1986, V001T01A058, http://dx.doi.org/10.1115/86-GT-144.
[22] B. Rosic, J.D. Denton, G. Pullan, The importance of shroud leakage modeling in multistage turbine flow calculations, ASME J. Turbomach. 128 (4) (2005) 699–707, https://doi.org/10.1115/1.2181999, 09.
[23] E.M. Greitzer, C.S. Tan, M.B. Graf, Internal Flow: Concepts and Applications, third ed., Cambridge University Press, Cambridge, 2007.
[24] J.D. Denton, L. Xu, The trailing edge loss of transonic turbine blades, ASME J. Turbomach. 112 (2) (1990) 277–285, https://doi.org/10.1115/1.2927648, 04.
[25] A.C. Senior, R.J. Miller, A data-centric approach to loss mechanisms, ASME J. Turbomach. 146 (4) (2023) 041007, https://doi.org/10.1115/1.4064167, 12.
[26] N.A. Cumpsty, Compressor Aerodynamics, Krieger Publishing, Florida, 2004.
[27] F. Tosto, A. Wheeler, M. Pini, Investigation of non-ideal effects in compressible boundary layers of dense vapors through direct numerical simulations, Phys. Fluids 36 (1) (2024) 016145, http://dx.doi.org/10.1063/5.0179570, 01.
[28] J. Szargut, D. Morris, F. Steward, Exergy Analysis of Thermal, Chemical, and Metallurgical Processes, Hemisphere Publishing Corporation, 1988.
[29] C. Michalakakis, J. Fouillou, R.C. Lupton, A. Gonzalez Hernandez, J.M. Cullen, Calculating the chemical exergy of materials, J. Ind. Ecol. 25 (2) (2021) 274–287, http://dx.doi.org/10.1111/jiec.13120.